Fault detection for LTI systems using data-driven dissipativity analysis

Rosa, Tábitha E.; de Paula Carvalho, Leonardo; Gleizer, Gabriel A.; Jayawardhana, Bayu

DOI
10.1016/j.mechatronics.2023.103111

Publication date
2024

Document Version
Final published version

Published in
Mechatronics

Mechatronics 97 (2024) 103111

Contents lists available at ScienceDirect

Mechatronics

journal homepage: www.elsevier.com/locate/mechatronics

Fault detection for LTI systems using data-driven dissipativity analysis ☆

Tábitha E. Rosa [a,*], Leonardo de Paula Carvalho [b], Gabriel A. Gleizer [c], Bayu Jayawardhana [a]

[a] ENgineering and TEchnology Institute Groningen (ENTEG), University of Groningen, Nijenborgh 4, Groningen, 9747 AG, The Netherlands
[b] Departamento de Engenharia de Telecomunicações e Controle, Universidade de São Paulo, Av. Prof. Luciano Gualberto, travessa 3, 58, São Paulo, 05508-900, SP, Brazil
[c] Delft Center for Systems and Control, Technology University of Delft, Mekelweg 2, Delft, 2628 CD, The Netherlands

ARTICLE INFO

Keywords:
Fault detection
Data-driven
Dissipativity
LTI systems
Model-free

ABSTRACT

Motivated by the physical exchange of energy and its dissipation in electro-mechanical systems, we propose a new fault detection method based on data-driven dissipativity analysis. We first identify a dissipativity inequality using one or multiple shots of data obtained from a linear time-invariant system. This dissipativity inequality's storage and supply rate functions assume generic quadratic difference forms encompassing all LTI systems. By analysing the norm of the identified dissipative inequality as the residual function, we can detect the occurrence of faults in real-time without the need to model each fault the system is subjected to. Through academic examples, we demonstrate how we can identify supply rate and storage functions from persistently exciting data shots. We present a practical example of detecting faults on a two-degree-of-freedom planar manipulator with zero missed fault detection rate, which is compared to a standard PCA-based fault detection algorithm.

1. Introduction

The second law of thermodynamics dictates that all physical processes have a finite lifetime and are subject to faults that can be attributed to fatigue accumulation and irreversible degradation processes in some parts of the systems. These problems can be fixed *a posteriori* by replacing the faulty components or be circumvented by performing predictive maintenance operations based on the *a priori* knowledge of the systems' state. Especially in complex and advanced systems, such as chemical plants, aircraft, production lines, railway networks and integrated systems, having a real-time system monitoring process has become critical.

In this context, timely and accurate fault diagnosis is essential for maintaining a healthy and operational system. The main fault detection problem consists of promptly determining when a dynamical system starts deviating from its nominal dynamical behaviour. A fault can be driven by, e.g., changes in system parameters, failures on sensors or actuators, or unexpected external disturbances influencing the system. There are many approaches to dealing with faults in the literature, and we refer to the works in [1–4], among others, that present most of the main well-established techniques.

In the fault diagnosis literature, it is common to deploy fault diagnosis systems using either a model describing the systems' dynamics or machine learning methods based on several batches of data from the systems [1,5,6]. However, with the increasing complexity of high-tech systems, the resulting complex models impede the deployment of model-based fault detection methods. At the same time, standard data-driven machine learning techniques are oblivious to fundamental mathematical properties that most physical systems possess, failing to achieve satisfactory results or requiring impractical amounts of data. As a hybrid approach, we present and use a behaviour-based fault detection method in this paper, where we monitor physics-informed systems' behaviour, such as dissipativity and passivity, which can be linked to the exchange of energy internally and externally with the environment. The energy interpretation of the method fits well with the law of degradation of energy from the second law of thermodynamics, as mentioned before.

Dissipativity theory was introduced by Willems [7], allowing the analysis of systems' dynamical behaviour via an energy dissipativity inequality defined by the input–output behaviours. The dissipativity inequality describes how the systems exchange their stored energy with the environment and dissipate it internally. Data-driven behavioural methods for establishing stability, passivity and dissipativity have been recently explored in control and fault diagnosis areas [8–12].

The application of dissipative systems theory for fault diagnosis was first proposed in [13], where the authors rely on the knowledge of the model to obtain the dissipativity inequality for fault diagnosis, and

☆ This paper was recommended for publication by Associate Editor Huihui Pan.

* Corresponding author.
E-mail addresses: tabithaesteves@gmail.com (T.E. Rosa), eng.leonardocarvalho@gmail.com (L. de Paula Carvalho), g.gleizer@tudelft.nl (G.A. Gleizer), b.jayawardhana@rug.nl (B. Jayawardhana).

https://doi.org/10.1016/j.mechatronics.2023.103111
Received 10 January 2023; Received in revised form 24 September 2023; Accepted 22 November 2023
Available online 27 November 2023

it is extended in [8,9,14] to the context of data-driven approach and learning method. The central point in [8,9,13] is to identify multiple dissipativity inequalities corresponding to the nominal system and each known fault. Accordingly, based on the obtained data-driven dissipative inequalities of various scenarios, they can be used online to test which scenario fits the measured data.

In contrast to the methods mentioned above, we present a data-driven method that can detect a fault based on observing a single dissipativity inequality, in which we follow a similar procedure as the one presented in [14]. While the method is not applicable for *fault isolation*, which is the case in [8,9,13], it allows for the detection of a fault in a simple way, without the need of building extensive knowledge of all possible faults that can occur. Particularly, in the development and deployment of customized high-tech systems, the occurrence of faults may not be known apriori during the design phase, and the demand for short time-to-market means that lifetime testing and characterization may not be performed extensively.

For data-driven identification and verification of dissipativity properties, we refer to recent works in [9,15–17]. The authors in [15] present a data-driven method to verify the standard QSR-dissipativity using one shot of data. In this case, the QSR-dissipativity is given by a quadratic supply-rate function encompassing passivity and ℓ_2-stability. Specifically, the supply-rate function uses the input and output signals at the current time with no dependence on the past time. As a generalization of this standard supply-rate function, the *Quadratic Difference Forms* (QdF) [18] can be used, taking past values into account. In fact, QdFs can be used to describe dissipativity of all linear systems [19]. QdF supply-rate functions have been used in data-driven dissipativity verification methods in [16,17]. However, in those works, the dissipativity is verified with only the supply-rate function without identifying the corresponding energy storage functions. Thus, using such methods in the fault detection context could lead to less accuracy in analysing the system's nominal dynamics. In [8,9,13,14], the authors point out that QdF-based dissipativity can provide more details of the process dynamic than the traditional sense, which helps improve the fault detection procedure.

Note also that a few methods were introduced in recent literature to obtain the so-called *L-QSR-dissipativity*. These approaches correspond to the verification of the QSR-dissipativity over a defined time-horizon [14,16,17,20]. In the present paper, differently from the methods above, we verify the infinite time-horizon approach that consists of the QSR-dissipativity, which is also investigated in [9]. While the authors in [9] apply the weaving response lemma concept to verify the dissipativity using a QdF form of both supply rate and storage functions, we extend the concepts introduced in [15] for a dissipative inequality written in terms of QdF supply rate form and standard energy storage functions, that is, depending on the state information. In the approach proposed in [15], which we extend in this paper, by applying the concept of Willems' fundamental lemma [21] and the definition of lag [15], the state of an LTI system can be rewritten as the extended state composed by inputs and outputs. In this way, by using the usual state-dependent storage function, the technique can also be further extended to deal with classical state-space approaches based on dissipativity properties.

Another important feature we cover in this paper is the use of multiple data shots in identifying a dissipativity inequality. This is particularly important in cases where the available data is not persistently exciting. Examples of these cases are those where it is impossible to perform several experiments to obtain the data, as in the ultra-high vacuum chemical vapour deposition processes described in [22], or when there are missing data in the available data. To solve this issue, the notion of collective persistence of excitation was proposed in [23], which is later used in [17] to verify the dissipativity of an LTI system.

Using the development in data-driven dissipativity analysis and verification described above, we present a fault detection method in this paper based on a data-driven dissipativity approach with QdF supply-rate and energy storage functions. We summarize the main contributions of this paper as follows:

- A method for the dissipativity analysis using a QdF supply-rate and standard energy storage functions;
- Verification of dissipativity using both one shot of persistently exciting input data and using multiple shots of collectively exciting input data coming from LTI systems;
- Data-driven fault detection method based on the use of the single dissipativity inequality identified in the previous step;
- Academic examples and an experimental result using a two-degree-of-freedom planar manipulator.

Notation. The set of vectors (matrices) of order n ($n \times m$) with real entries is represented by $\mathbb{R}^n$ ($\mathbb{R}^{n\times m}$) and correspondingly, that with integer entries is denoted by $\mathbb{Z}^n$ ($\mathbb{Z}^{n\times m}$). Similar notation is applied to denote a vector (matrix) with zeros and ones by 0^n and 1^n (or $0^{n\times m}$ and $1^{n\times m}$), respectively. I^n denotes the $n\times n$ identity matrix. Additionally, we use a subscript + to denote sets with only positive entries, for instance, $\mathbb{Z}_+$ that denotes a set of positive integers. For matrices or vectors, the symbol $^\top$ denotes the transpose. A positive definite symmetric matrix P is denoted by $P \succeq 0$. The space of square-summable discrete-time signals is denoted by $\ell_2(\mathbb{R}^\bullet)$. Given $e \in \ell_2(\mathbb{R}^\bullet)$, we denote $\{e\}_i^j = \{e(i), \dots, e(j)\}$ and we define its stacked vector by

$$e_{[i,j]} = \begin{bmatrix} e(i)^\top & e(i+1)^\top & \cdots & e(j)^\top \end{bmatrix}^\top. \tag{1}$$

Throughout the paper, we use them interchangeably whenever it is clear from the context.

A Hankel matrix with $L \in \mathbb{Z}_+$ block rows of a finite sequence $e_{[0,T-1]}$ is given by

$$H_L(e_{[0,T-1]}) = \begin{bmatrix} e(0) & e(1) & \cdots & e(T-L) \\ e(1) & e(2) & \cdots & e(T-L+1) \\ \vdots & \vdots & \ddots & \vdots \\ e(L-1) & e(L-2) & \cdots & e(T-1) \end{bmatrix}. \tag{2}$$

Definition 1 (*[21]*)**.** A measured trajectory $e_{[0,T-1]}$, $e : \mathbb{Z} \to \mathbb{R}^n$ is *persistently exciting* of order L if $\operatorname{rank}(H_L(e_{[0,T-1]})) = nL$.

2. Dissipativity analysis

In this paper, we analyse the following discrete-time linear time-invariant (LTI) system

$$\Sigma : \begin{cases} x(k+1) = Ax(k) + Bu(k), \\ y(k) = Cx(k) + Du(k), \\ x(0) = x_0, \end{cases} \tag{3}$$

where $x(k) \in \mathbb{R}^n$, $u(k) \in \mathbb{R}^m$ and $y(k) \in \mathbb{R}^p$ are, respectively, the state vector, the control input and the output of the system. We assume that $u \in \ell_2(\mathbb{R}^m)$ and the state-space matrices are assumed to be the minimal realization of system Σ. Furthermore, we consider the case where the state-space matrices are unknown, but the inputs and outputs are available for all $k = 0, \dots, T_f$, with T_f being any arbitrary given time.

Definition 2. System (3) is said to be *dissipative* with respect to a *supply-rate* operator $w : \ell_2(\mathbb{R}^m) \times \ell_2(\mathbb{R}^p) \times \mathbb{Z}_+ \to \mathbb{R}$ if there exists a *storage function* $V : \mathbb{R}^n \to \mathbb{R}_+$ with $V(0) = 0$ such that

$$V(x(k+1)) - V(x(k)) \le w(y, u, k) \tag{4}$$

holds along all possible trajectories of (3) for all $k \ge 0$, (x, y, u) satisfying (3) and $u \in \ell_2(\mathbb{R}^m)$. This definition can be found in detail in [7,24].

Regarding the supply rate function/operator w, as used in [8,16,19], we consider the quadratic difference forms (QdF) as follows

$$\begin{aligned} &w(y_{[k,k+N]}, u_{[k,k+N]}) \\ &\quad = \sum_{i,j=0}^{N} \begin{bmatrix} y(k+i) \\ u(k+i) \end{bmatrix}^\top \begin{bmatrix} Q_{ij} & S_{ij} \\ S_{ij}^\top & R_{ij} \end{bmatrix} \begin{bmatrix} y(k+j) \\ u(k+j) \end{bmatrix}, \\ &\quad = \begin{bmatrix} y_{[k,k+N]} \\ u_{[k,k+N]} \end{bmatrix}^\top \begin{bmatrix} Q & S \\ S^\top & R \end{bmatrix} \begin{bmatrix} y_{[k,k+N]} \\ u_{[k,k+N]} \end{bmatrix}, \end{aligned} \tag{5}$$

for every $k \geq N$, where each Q_{ij}, S_{ij} and R_{ij} are part of the usual QSR matrix and $Q_{ij} = Q_{ij}^{\top}$ and $R_{ij} = R_{ij}^{\top}$ and

$$\Phi = \begin{bmatrix} Q & S \\ S^{\top} & R \end{bmatrix}.$$

Similarly, for the construction of the energy storage function V, we assume that it is given by

$$V(x(k)) = x(k)^{\top} P' x(k), \tag{6}$$

where $P' = P'^{\top} \geq 0$ and $P' \in \mathbb{R}^{n \times n}$.

2.1. Dissipativity analysis via one-shot of data

In order to verify the dissipativity inequality (4) from the available data, the well-known Willem's fundamental lemma [21, Theorem 1] on persistence of excitation has become an essential tool. This lemma, which we recall in Definition 1, states that all possible trajectories $(\bar{y}_{[0,L-1]}, \bar{u}_{[0,L-1]})$ of System (3) can be obtained from a single trajectory whose input is persistently exciting.

Lemma 1 (*[21]*). *Suppose that* $\begin{bmatrix} y_{[0,T-1]} \\ u_{[0,T-1]} \end{bmatrix}$ *is a trajectory of* Σ *where* $u_{[0,T-1]}$ *is persistently exciting of order* $L+n$. *Then* $(\bar{y}_{[0,L-1]}, \bar{u}_{[0,L-1]})$ *is an admissible trajectory of* Σ *if and only if there exists a vector* $\alpha \in \mathbb{R}^{T-L+1}$ *such that*

$$\begin{bmatrix} H_L(y_{[0,T-1]}) \\ H_L(u_{[0,T-1]}) \end{bmatrix} \alpha = \begin{bmatrix} \bar{y}_{[0,L-1]} \\ \bar{u}_{[0,L-1]} \end{bmatrix}. \tag{7}$$

This lemma is supported by the concept of lag of a system, also introduced in [21], using the behavioural framework. In [15], the authors introduce a well-defined definition of lag in the context of state-space systems. This definition is presented as follows.

Lemma 2 (*[15]*). *The lag* $\underline{L}$ *of system (3) is the smallest* $L \in \mathbb{Z}_+$ *such that the observability matrix* $\mathcal{O}_L = [\, C^{\top} \ (CA)^{\top} \ \cdots \ (CA^{L-1})^{\top} \,]^{\top}$ *has rank n.*

Now, using this concept and as discussed in detail in [15], we have that, given $L \geq \underline{L}$ and a set of data $\{y, u\}_{[0,T-1]}$ obtained from (3), we can rewrite system (3) using an extended state

$$\xi(k) = \begin{bmatrix} y_{[k-L,k-1]} \\ u_{[k-L,k-1]} \end{bmatrix}. \tag{8}$$

This extended system is given by

$$\begin{aligned} \xi(k+1) &= \tilde{A}\xi(k) + \tilde{B}u(k), \\ y(k) &= \tilde{C}\xi(k) + \tilde{D}u(k), \end{aligned} \tag{9}$$

with existing initial condition ξ_0 and matrices $\tilde{A}$, $\tilde{B}$, $\tilde{C}$ and $\tilde{D}$ obtained directly from the measured set of data $\{u, y\}_{[0,T-1]}$. Another critical point to highlight is that using the measured set of data with the input being persistently exciting, we can map the state x from ξ via $x(k) = M\xi(k)$ where M can be constructed directly from the data. For the sake of simplicity, we refer interested readers to [15].

Let us now state our first problem that will be tackled in this paper as follows.

***QdF*-dissipativity verification problem:** For a trajectory $(y_{[0,T-1]}, u_{[0,T-1]})$ of Σ, $L \geq \underline{L}$ and the input being persistently exciting of order $L + N + n + 1$, verify if there exists a symmetric matrix $P = P^{\top} \geq 0$, $P \in \mathbb{R}^{(m+p)L \times (m+p)L}$ and $P = M^{\top} P' M$ such that

$$V(\xi(k+1)) - V(\xi(k)) \leq w(y_{[k,k+N]}, u_{[k,k+N]}) \tag{10}$$

holds for $\xi_0 \in \mathbb{R}^{(m+p)L}$ with

$$V(\xi(k)) = \xi(k)^{\top} P \xi(k), \tag{11}$$

and w be as in (5).

In order to accommodate the presentation of our first main result, let us introduce the following notations.

$$\begin{aligned} Z(k) &= \begin{bmatrix} y(k)^{\top} & \cdots & y(k+N)^{\top} & u(k)^{\top} & \cdots & u(k+N)^{\top} \end{bmatrix}^{\top}, \\ U(k) &= \begin{bmatrix} u(k)^{\top} & \cdots & u(k+N)^{\top} \end{bmatrix}^{\top}, \\ \Xi_k &= \begin{bmatrix} H_L(y_{[k,T-2+k]}) \\ H_L(u_{[k,T-2+k]}) \end{bmatrix}. \end{aligned} \tag{12}$$

Theorem 1. *Let* $(y_{[0,T+N-1]}, u_{[0,T+N-1]})$ *be a trajectory of (3), where* $u_{[0,T+N-1]}$ *is persistently exciting of order* $L + N + n + 1$, *and* $L \geq \underline{L}$. *If there exists a matrix* $P = P^{\top} \geq 0$ *such that*

$$\Xi_1^{\top} P \Xi_1 - \Xi_0^{\top} P \Xi_0 - Z_{[L,T-1]}^{\top} \Phi Z_{[L,T-1]} \preceq 0 \tag{13}$$

holds, then (3) is QSR-dissipative.

Proof. In Theorem 1 we want to verify the dissipative inequality in (4), which can be rewritten as

$$\begin{aligned} x(k+1)^{\top} P' x(k+1) - x(k)^{\top} P' x(k) \leq \\ \begin{bmatrix} y_{[k,k+N]} \\ u_{[k,k+N]} \end{bmatrix}^{\top} \Phi \begin{bmatrix} y_{[k,k+N]} \\ u_{[k,k+N]} \end{bmatrix}, \end{aligned} \tag{14}$$

which holds for all $k \geq 0$, with $x(0) = x_0$, and $P' = P'^{\top} \geq 0$. When $L \geq \underline{L}$, the system (3) can be rewritten as (9) using the extended state ξ. Subsequently, we can rewrite the dissipativity inequality as

$$\begin{aligned} \xi(k+1)^{\top} P \xi(k+1) - \xi(k)^{\top} P \xi(k) \leq \\ \begin{bmatrix} y_{[k,k+N]} \\ u_{[k,k+N]} \end{bmatrix}^{\top} \Phi \begin{bmatrix} y_{[k,k+N]} \\ u_{[k,k+N]} \end{bmatrix} \end{aligned} \tag{15}$$

which is equivalent to

$$\begin{aligned} \begin{bmatrix} y_{[k-L+1,k]} \\ u_{[k-L+1,k]} \end{bmatrix}^{\top} P \begin{bmatrix} y_{[k-L+1,k]} \\ u_{[k-L+1,k]} \end{bmatrix} - \begin{bmatrix} y_{[k-L,k-1]} \\ u_{[k-L,k-1]} \end{bmatrix}^{\top} P \begin{bmatrix} y_{[k-L,k-1]} \\ u_{[k-L,k-1]} \end{bmatrix} \\ \leq \begin{bmatrix} y_{[k,k+N]} \\ u_{[k,k+N]} \end{bmatrix}^{\top} \Phi \begin{bmatrix} y_{[k,k+N]} \\ u_{[k,k+N]} \end{bmatrix}. \end{aligned} \tag{16}$$

According to Lemma 1, if the input $u_{[0,T+N-1]}$ is persistently exciting of order $L+n$ then any other trajectory $(y_{[0,L-1]}, u_{[0,L-1]})$ can be obtained from the measured data. Looking at the extended system (9), we have that with the input being persistently exciting of order $L + n$, we can obtain the extended state-space matrices, such that we can rewrite (15) as

$$\begin{aligned} \begin{bmatrix} \xi(k) \\ u(k) \end{bmatrix}^{\top} \begin{bmatrix} \tilde{A}^{\top} P \tilde{A} - P & \star \\ \tilde{B}^{\top} P \tilde{A} & \tilde{B}^{\top} P \tilde{B} \end{bmatrix} \begin{bmatrix} \xi(k) \\ u(k) \end{bmatrix} \leq \\ \begin{bmatrix} \xi_{[k,k+N]} \\ u_{[k,k+N]} \end{bmatrix}^{\top} \begin{bmatrix} \Pi_{11} & \star \\ \Pi_{12} & \Pi_{22} \end{bmatrix} \begin{bmatrix} \xi_{[k,k+N]} \\ u_{[k,k+N]} \end{bmatrix} \end{aligned} \tag{17}$$

with

$$\begin{aligned} \Pi_{11} &= \tilde{C}^{\top} Q \tilde{C}, \quad \Pi_{12} = S^{\top} \tilde{C} + \tilde{D}^{\top} Q \tilde{C}, \\ \Pi_{22} &= \tilde{D}^{\top} Q \tilde{D} + \tilde{D}^{\top} S + S^{\top} \tilde{D} + R, \end{aligned}$$

and $\tilde{C} = \tilde{C} \otimes I_N$, $\tilde{D} = \tilde{D} \otimes I_N$.

Moreover, when the input is persistently exciting of order $L+n$, the Hankel matrix $\begin{bmatrix} H_L(y_{[0,T-1]}) \\ H_L(u_{[0,T-1]}) \end{bmatrix}$ is full row rank, which spans all possible trajectories $(\bar{y}_{[0,L-1]}, \bar{u}_{[0,L-1]})$ of inputs and outputs of this system. Recall that

$$\begin{aligned} \begin{bmatrix} H_L(y_{[0,T-1]}) \\ H_L(u_{[0,T-1]}) \end{bmatrix} &= \begin{bmatrix} \xi(L) & \xi(L+1) & \cdots & \xi(T-1) & \xi(T) \end{bmatrix}, \\ &= \begin{bmatrix} \Xi_0 & \xi(T) \end{bmatrix} = \begin{bmatrix} \xi(L) & \Xi_1 \end{bmatrix}. \end{aligned} \tag{18}$$

Using this relation, if the input is persistently exciting of order $L + n$ we have that both Ξ_0 and Ξ_1 span all reachable states of the extended system (9). Now, if $u_{[0,T-1]}$ is persistently exciting of order $L + n + 1$, then $\begin{bmatrix} H_{L+1}(y_{[0,T-1]}) \\ H_{L+1}(u_{[0,T-1]}) \end{bmatrix}$ has full row rank and, from this result, we have that

$$\begin{bmatrix} \Xi_0 \\ u_{[L,T-1]}^{\top} \end{bmatrix}$$

spans all input-state trajectories of the extended system.

However, note that we also need to guarantee all possible input-state trajectories to verify the supply function. This can be achieved if we consider the input $u_{[0,T+N-1]}$ being persistently exciting of order $L + N + n + 1$, which guarantees that

$$\begin{bmatrix} H_{L+N}(y_{[0,T+N-2]}) \\ H_{L+N}(u_{[0,T+N-2]}) \\ U_{[L,T-1]}^{\top} \end{bmatrix}$$

spans all input-state trajectories of the extended system for all the trajectories $(\bar{y}_{[0,L+N-1]}, \bar{u}_{[0,L+N-1]})$ with $U_{[L,T-1]}$ be defined as in (1) and $U(k)$ as in (12). Note that $\Xi_{[0,N]}$ and $\begin{bmatrix} H_{L+N}(y_{[0,T+N-2]}) \\ H_{L+N}(u_{[0,T+N-2]}) \end{bmatrix}$ are similar, since the former is a rearrangement of the same elements contained on the latter, i.e., they are related by a permutation matrix. Thus, we have that

$$\begin{bmatrix} \Xi_{[0,N]} \\ U^{\top}_{[L,T-1]} \end{bmatrix}$$

also spans all input-state trajectories of the extended system for all the trajectories $(\bar{y}_{[0,L+N-1]}, \bar{u}_{[0,L+N-1]})$.

Thus, we can rewrite (17) in terms of the available data, that is

$$\begin{bmatrix} \Xi_0 \\ u^{\top}_{[L,T-1]} \end{bmatrix}^{\top} \begin{bmatrix} \tilde{A}^{\top} P \tilde{A} - P & \star \\ \tilde{B}^{\top} P \tilde{A} & \tilde{B}^{\top} P \tilde{B} \end{bmatrix} \begin{bmatrix} \Xi_0 \\ u^{\top}_{[L,T-1]} \end{bmatrix} \preceq \begin{bmatrix} \Xi_{[0,N]} \\ U^{\top}_{[L,T-1]} \end{bmatrix}^{\top} \begin{bmatrix} \Pi_{11} & \star \\ \Pi_{12} & \Pi_{22} \end{bmatrix} \begin{bmatrix} \Xi_{[0,N]} \\ U^{\top}_{[L,T-1]} \end{bmatrix}, \tag{19}$$

with the same matrices Π_{ij}, $i, j = \{1, 2\}$ as before.

Therefore, the existence of a matrix $P = P^{\top} \succeq 0$ such that (19) holds, implies that the system is dissipative with respect to the supply rate w.

Now we prove the converse result. If system (3) is dissipative with respect to the supply rate w with a storage function given by $V(x(k)) = x(k)^{\top} P' x(k)$, a combination of the results in [19,25] gives that the following inequality holds for all of its state-input trajectories:

$$\begin{bmatrix} x(k) \\ u(k) \end{bmatrix}^{\top} \begin{bmatrix} A^{\top} P A - P & \star \\ B^{\top} P A & B^{\top} P B \end{bmatrix} \begin{bmatrix} x(k) \\ u(k) \end{bmatrix} \preceq \begin{bmatrix} x_{[k,k+N]} \\ u_{[k,k+N]} \end{bmatrix}^{\top} \begin{bmatrix} \Pi'_{11} & \star \\ \Pi'_{12} & \Pi'_{22} \end{bmatrix} \begin{bmatrix} x_{[k,k+N]} \\ u_{[k,k+N]} \end{bmatrix}, \tag{20}$$

with

$$\Pi'_{11} = C^{\top} Q C, \quad \Pi'_{12} = S^{\top} C + \mathcal{D}^{\top} Q C,$$
$$\Pi'_{22} = \mathcal{D}^{\top} Q \mathcal{D} + \mathcal{D}^{\top} S + S^{\top} \mathcal{D} + R,$$

and $C = C \otimes I_N$, $\mathcal{D} = D \otimes I_N$. Since we know from Lemmas 1 and 2 that there is a matrix M such that $x(k) = M\xi(k)$, we can obtain (19) from (20). □

Note that when we apply Theorem 1 with a supply function (5) with $N = 0$, we recover the results given in [15, Theorem 5]. This means that such conditions are included in Theorem 1, but not the opposite. As we have mentioned in the introduction, the main advantages of using a supply-rate with a QdF formulation, that is, $N \geq 0$, are that we can describe the dissipativity of all linear systems [19]. Also, in the context of fault detection, this formulation can provide more insights into the systems' dynamics, which leads to a better fault detection method [8].

2.2. Dissipativity analysis via multiple shots of data

In the previous section, we have dealt with the case of one shot of measured data $\{y, u\}_{[0,T-1]}$ that is sufficient to describe the dynamical behaviour of the system. However, in practice, finding such batch of data is not always possible. We can have cases, for instance, where we have corrupted or missing data or even an insufficient amount of data that may not satisfy the persistence of the excitation condition given in Lemma 1. One approach to deal with such cases is using the *collective persistence of excitation* concept [23], defined as follows.

Definition 3 ([23]). Consider a set of q measured trajectories given by $\mathbf{e}_{[0,\mathbf{T}-1]} := \left\{ e^1_{[0,T_1-1]}, e^2_{[0,T_2-1]}, \dots, e^q_{[0,T_q-1]} \right\}$, $e^i : \mathbb{Z} \to \mathbb{R}^n$, where $L \leq T_i$ holds for a positive integer L and for all i. This set of trajectories is *collectively persistently exciting* of order L if the following mosaic-Hankel matrix

$$\mathcal{H}_L(\mathbf{e}_{[0,\mathbf{T}-1]}) = \begin{bmatrix} H_L(e^1_{[0,T_1-1]}) & H_L(e^2_{[0,T_2-1]}) & \cdots & H_L(e^q_{[0,T_q-1]}) \end{bmatrix} \tag{21}$$

has full row rank.

Using this notion, a set of measured trajectories with possible different lengths can be used together to obtain every possible trajectory of Σ with a time horizon L, as given in the following lemma.

Lemma 3 ([23]). *Let $\left(y^i_{[0,T_i+N-1]}, u^i_{[0,T_i+N-1]}\right)$, $i = 1, \dots, q$, be trajectories of Σ, with $L \leq T_i$ for all i for some $L > 0$. If the set of inputs $u^i(k)$ is collectively persistently exciting of order $L + n$, then $\left(\bar{y}_{[0,L-1]}, \bar{u}_{[0,L-1]}\right)$ is an admissible trajectory of (3) if and only if there exists a vector α with appropriate dimension such that*

$$\begin{bmatrix} \mathcal{H}_L\left(\mathbf{y}_{[0,\mathbf{T}-1]}\right) \\ \mathcal{H}_L\left(\mathbf{u}_{[0,\mathbf{T}-1]}\right) \end{bmatrix} \alpha = \begin{bmatrix} \bar{y}_{[0,L-1]} \\ \bar{u}_{[0,L-1]} \end{bmatrix}, \tag{22}$$

where the matrices on the left side are mosaic-Hankel matrices as in (21).

Accordingly, we can define the following data-driven dissipativity verification problem.

***QSR*-dissipativity verification problem for multiple shots of data:** For given multiple shots of trajectories $\left(y^i_{[0,T_i]}, u^i_{[0,T_i]}\right)$, $T_i > 0$, $i = 1, \dots, q$ of Σ, where $L \geq \underline{L}$ and the set of inputs $u^i_{[0,T_i+N-1]}$, $i = 1, \dots, q$, is collectively persistently exciting of order $L + N + n + 1$, verify if there exists a symmetric matrix $P = P^{\top} \succeq 0$, $P \in \mathbb{R}^{(m+p)L \times (m+p)L}$ and $P = M^{\top} P' M$ such that (15) holds for $\xi_0 \in \mathbb{R}^{(m+p)L}$ with the storage function as in(11) and the supply-rate $w(y(k), u(k))$ as in (5).

Before we introduce our next result, let us introduce the following notations

$$\mathbf{Z} = \begin{bmatrix} Z^1_{[L,T-1]} & \cdots & Z^q_{[L,T-1]} \end{bmatrix}, \quad \Xi_k = \begin{bmatrix} \mathcal{H}_L\left(\mathbf{y}_{[k,\mathbf{T}-2+k]}\right) \\ \mathcal{H}_L\left(\mathbf{u}_{[k,\mathbf{T}-2+k]}\right) \end{bmatrix}, \tag{23}$$

where $Z^i(k)$ as described in (12) and $\mathcal{H}_L(\cdot)$ are Mosaic-Hankel matrices as in (21).

Corollary 1.

Let $L \geq \underline{L}$ and $\left(y^i_{[0,T_i+N-1]}, u^i_{[0,T_i+N-1]}\right)$, $T_i > 0$, $i = 1, \dots, q$ be a set of trajectories of (3) with n being the order of the system, with the set of inputs $u^i_{[0,T_i+N-1]}$, $i = 1, \dots, q$, being collectively persistently exciting of order $L + N + n + 1$. If there exists a matrix $P = P^{\top} \succeq 0$ such that

$$\Xi_1^{\top} P \Xi_1 - \Xi_0^{\top} P \Xi_0 - \mathbf{Z}^{\top} \Phi \mathbf{Z} \preceq 0, \tag{24}$$

holds, then (3) is QSR-dissipative.

Proof. The proof of this theorem comes directly from the application of Lemma 3 on Theorem 1. This can be done by using the fact that

$$\begin{bmatrix} \mathcal{H}_{L+N+1}\left(\mathbf{y}_{[0,\mathbf{T}-1]}\right) \\ \mathcal{H}_{L+N+1}\left(\mathbf{u}_{[0,\mathbf{T}-1]}\right) \end{bmatrix}$$

spans the whole space of input–output trajectories. □

3. Fault detection

In this section, we will present the application of previous data-driven dissipativity analysis in fault detection. Let us consider again the LTI system described in (3) that is dissipative with respect to a supply rate w. Following Definition 2, when the system is dissipative, there exist $P \succ 0$ and Φ such that the dissipativity inequality (15) holds. Note that (15) can be rewritten into

$$Y(k) := V(\xi(k+1)) - V(\xi(k)) - w(y_{[k,k+N]}, u_{[k,k+N]}) \leq 0, \tag{25}$$

with $V(\xi(k)) = \xi(k)^{\top} P \xi(k)$ and w be as in (5) for all $k - L \geq 0$. Note that $k - L \geq 0$ is required given that $\xi(k)$ consists of the L past samples as shown in (8). We remark here that for an online approach, the time variable k may not correspond directly to the real time instant. In this case, the real time instant k' can, for instance, be related to $k' = k + N$.

When the dissipative system (3) operates normally, that is, without any faults, the inequality (25) holds for all trajectories. This inequality can be physically interpreted as an energy balance description of the system. The presence of a fault in the system can change the relation of energy exchange and dissipation. For example, a faulty spring-damper element will lead to a different dissipativity inequality than the nominal one. In this case, monitoring the energy dissipation relation (25) directly can be used as a fault detection method.

As discussed in the Introduction, such fault can have severe consequences for the safety of the operation when, e.g., the system is interconnected with others. Nonetheless, there are cases where the system may still be dissipative with respect to the nominal supply rate, but the energy balance does not follow the nominal values. Therefore, we propose using the signal Y in (25), which measures the change in the total energy balance of the system as a basis for a fault diagnosis function but not as a residual function itself.

Generally, a faulty system is described as the LTI systems (3) subjected to an unknown additive fault signal $f(k)$:

$$\Sigma : \begin{cases} x(k+1) = Ax(k) + Bu(k) + F_u f(k), \\ y(k) = Cx(k) + Du(k) + F_y f(k), \\ x(0) = x_0, \end{cases} \tag{26}$$

where F_u and F_y are matrices that describe how the fault affects the dynamics and the measurement, respectively. This general description accommodates different types of faults, for instance, $F_u = B$ represents actuator faults, and $F_y = C$ represents sensor faults. The fault detection problem is to determine online whether $f(k) \neq 0$ for some k.[1] As discussed at the beginning of this paper, we assume that we do not know all state-space matrices of the system, nor do we have direct access to $x(k)$. Thus, we propose a fault detection method that only observes the input and output signals.

Correspondingly, we consider the following residual function based on the dissipativity inequality (25)

$$J(k) = \sqrt{\sum_{i=k-T_F}^{k} Y^2(i)}, \tag{27}$$

that can be computed for any $k - T_F \geq 0$ and where $k \geq T_F$ does not include the transient data and T_F is the window of samples observed for detecting faults.

It is necessary to define a threshold[2] to detect the fault occurrence. The threshold definition is an important step in most fault detection approaches since it determines the rate of false alarms. In other words, the problem of detecting a fault is given by

$$\begin{aligned} &J(k) \leq \text{TH}, \text{ for } f(k) = 0, \\ &J(k) > \text{TH}, \text{ for } f(k) \neq 0, \end{aligned} \tag{28}$$

where TH is the threshold value.

Determining an effective threshold can be difficult, and there are multiple ways to do it [1]. In this paper, we propose two simple approaches based on the assumption that we are dealing with a LTI system without uncertainties.

Following the methodology in [1], the first method starts from verifying the largest magnitude value obtained for the residual function 27 in a fault-free trajectory. Then, we can set the threshold slightly larger than this value. In other words,

$$\text{TH}_\beta = \beta \max\{J_{[0,T_{\text{TH}}]}\}, \tag{29}$$

where $\beta > 0$, $T_{\text{TH}} \geq T_F$, and $[0, T_{\text{TH}}]$ is an interval of data that is fault-free and also contains the data used for the identification of the dissipative inequality (25).

Another way to define the threshold is to obtain the mean value of $J(k)$ using these samples and its standard deviation to obtain the threshold. In this case

$$\text{TH}_\gamma = \text{mean}(J_{[0,T_{\text{TH}}]}) + \gamma \ \text{std}(J_{[0,T_{\text{TH}}]}), \tag{30}$$

where mean is the time average of the observed trajectory and std is its standard deviation. The user-defined parameter γ is the Z-score, which dictates how much deviation is allowed before triggering a fault; e.g., under the assumption of $J_{[0,T_{\text{TH}}]}$ being normally distributed, $\gamma = 3$ would allow for 99.73% of the cases to be considered normal. Both parameters β and γ should be tuned to get an acceptable trade-off between false alarm rate with missed detection rate. Note that the choice of parameters β and γ are case-based and should be made by the user.

In Algorithm 1 below, we summarize the main procedure of fault detection using the dissipativity inequality identified in Section 2.

Algorithm 1 Fault detection online procedure.

Initialization: $\{y, u\}_{[k-L,k+N-1]}$ for each $k - L \geq 0$, scalars L, T, N, TH, matrices P and Φ

For each time instant k compute

$$Y(k) = \begin{bmatrix} y_{[k-L+1,k]} \\ u_{[k-L+1,k]} \end{bmatrix}^\top P \begin{bmatrix} y_{[k-L+1,k]} \\ u_{[k-L+1,k]} \end{bmatrix} - \begin{bmatrix} y_{[k-L,k-1]} \\ u_{[k-L,k-1]} \end{bmatrix}^\top P \begin{bmatrix} y_{[k-L,k-1]} \\ u_{[k-L,k-1]} \end{bmatrix} - \begin{bmatrix} y_{[k,k+N]} \\ u_{[k,k+N]} \end{bmatrix}^\top \Phi \begin{bmatrix} y_{[k,k+N]} \\ u_{[k,k+N]} \end{bmatrix}$$

$J(k) = \sqrt{\sum_{i=k-T_F}^{k} Y^2(i)}$

if $J(k) \leq \text{TH}$ **then**

$f(k) = 0$

else if $J(k) > \text{TH}$ **then**

$f(k) = 1$

end if

In this paper, we do not provide a method to establish and analyse the values of the fault signal $f(k)$. In Algorithm 1, we simply identify the presence of a fault by giving it a binary number where the presence of a fault is indicated as $f(k) = 1$ and the contrary $f(k) = 0$.

Remark 1. We treat the problem of fault detection in a *semi-supervised* learning framework. That is, we only assume to have data from controlled experiments (i.e., using persistently exciting input data) from the nominal system. Based only from this limited information, we construct the dissipativity function and the fault detection algorithm. We chose this approach because it is a common challenge in fault diagnosis to obtain data from faulty scenarios, especially because (i) it is difficult to anticipate all faults that can occur in a system, and (ii) it is often risky to operate a system in faulty conditions. This is in contrast to the methods that treat the problem of fault classification as a *multi-class supervised* learning problem, where there are $q+1$ modes (1 nominal and q faulty modes) that are known to exist, and one has data available for all of those q modes. In particular, the data available for the faulty modes has also persistently exciting input property, which means that potentially controlled experiments for the faulty modes are necessary. The advantage of the approach of [8,9,14] is that, *if* the data for all fault modes is available, the detection guarantees are stronger.

4. Simulation and experimental validation

In this section, we present numerical simulations for checking the QSR-dissipativity and experimental results on dissipativity analysis and its use for data-driven fault detection using a two-degree-of-freedom (DoF) planar manipulator.

[1] No assumption is made on whether or not f is independent of x. To represent changes in parameters in A, we have so-called multiplicative faults, i.e., $f_i(k) = w_i(k)x_i(k)$, where $w(k)$ is taken as an unknown signal. Clearly, if $x(k) \neq 0$, that is, the system is not resting in equilibrium, then $f(k) = 0$ only if $w(k) = 0$, which is the faultless case.

[2] Here, a *threshold* refers to the value of $J(k)$ corresponding to the boundary of fault occurrence when it is surpassed.

For the simulation setup, we use the numerical software Matlab (R2022a) in conjunction with the parser YALMIP [26] and the solver Mosek [27] for the optimization procedures of finding feasible solutions for Theorem 1 via linear matrix inequality (LMI) conditions.

4.1. Dissipativity of a mass–spring–damper system

Consider the classic mass–spring–damper system based on Example 6.4 from [19]. This example has also been explored in [16] in the context of data-driven dissipative analysis where the QSR-dissipativity is verified using a one-shot of data. We assume that the following state-space describes its dynamics

$$\begin{aligned} x(k+1) &= \begin{bmatrix} 0 & 1 \\ -K & -D \end{bmatrix} x(k) + \begin{bmatrix} 0 \\ 1 \end{bmatrix} u(k), \\ y(k) &= \begin{bmatrix} 1 & 0 \end{bmatrix} x(k), \end{aligned} \tag{31}$$

which can also be described in terms only of the inputs and outputs, that is

$$y(k+2) + Dy(k+1) + Ky(k) = u(k). \tag{32}$$

In this paper, we assume $K = D = 1$. Additionally, we consider the trajectories computed in [16], where different batches of data are generated using zero initial conditions and a normally distributed input with a standard deviation of 10 and zero mean. For the verification of dissipativity, we consider $L = 2$, $N = 1$, and $T = (m+1)(L+n)+m(N+1) = 10$, which guarantees that the set of data is persistently exciting. The choice of $L = 2$ comes from $\underline{L} \leq n \leq L$, and that $n = 2$.

In this example, we consider three cases for verifying the QSR-dissipativity. We apply one shot of data from the available measurements for all three cases.

The first case we tackle is where both the supply rate and the storage functions, Φ and P, respectively, are unknown and based on a single trajectory, and we use Theorem 1 for their search. We can apply the procedure for the first case using the information above. As expected, since we already know that the system is dissipative, we can find both matrices Φ and P, which are given as follows

$$\Phi = \begin{bmatrix} -4.3345 & -2.1746 & -2.1826 & 0.0044 \\ -2.1746 & 2.1614 & -0.0084 & 0.0029 \\ -2.1826 & -0.0084 & -2.1100 & -0.0132 \\ 0.0044 & 0.0029 & -0.0132 & 4.3495 \end{bmatrix},$$

$$P = \begin{bmatrix} 2.1823 & 0.0037 & -2.1834 & 0.0033 \\ 0.0037 & 4.3429 & -0.0090 & 0.0017 \\ -2.1834 & -0.0090 & 2.2191 & -0.0083 \\ 0.0033 & 0.0017 & -0.0083 & 4.3426 \end{bmatrix}.$$

Note that both Φ and P are symmetric and $P \succeq 0$, as required in Theorem 1.

For the second case, we can consider a storage function V that depends only on the outputs $(y(k), y(k+1))$, the same way as proposed in [16]. Writing the storage function in terms of the extended state $\xi(k)$, we obtain

$$V(k) = \xi(k)^\top \begin{bmatrix} 10 & 0 & 0 & \\ 0 & 1 & 0 & 0 \\ 0 & 0 & 0 & 0 \\ 0 & 0 & 0 & 0 \end{bmatrix} \xi(k), \tag{33}$$

from which we can recover the respective matrix P and apply it as an input to the optimization problem. Thus, we can apply Theorem 1 searching for an existing matrix Φ. We can find such a suitable supply rate, which is given as follows

$$\Phi = \begin{bmatrix} 1.0378 & 0.9091 & -2.9291 & 2.2938 \\ 0.9091 & 2.7223 & -5.1728 & 2.5707 \\ -2.9291 & -5.1728 & 26.5080 & -10.0341 \\ 2.2938 & 2.5707 & -10.0341 & 14.2297 \end{bmatrix}.$$

Now, for the last case, we consider the knowledge of the supply rate w *a priori*, and we search for the matrix P. We know from [16], that a suitable supply rate for system (32) is as follows

$$\begin{aligned} w(y(k), u(k)) &= u^2(k) - 2y(k)u(k) - 2y(k+1)u(k) \\ &\quad +2y(k)y(k+1) + y(k+1)^2, \end{aligned}$$

which, based on (5) with $N = 1$, can be rearranged using

$$\Phi_{00} = \begin{bmatrix} 0 & 1 \\ 1 & 1 \end{bmatrix}, \ \Phi_{01} = \begin{bmatrix} -1 & 0 \\ -1 & 0 \end{bmatrix}, \ \Phi_{11} = \begin{bmatrix} 1 & 0 \\ 0 & 0 \end{bmatrix}. \tag{34}$$

We can use this matrix on the problem and then search for a suitable storage function. By doing so, we obtain the following matrix

$$P = \begin{bmatrix} 1 & 1 & -1 & 0 \\ 1 & 2 & -1 & 0 \\ -1 & -1 & 1 & 0 \\ 0 & 0 & 0 & 0 \end{bmatrix},$$

which, as expected, holds with the requirements of $P \succeq 0$.

4.2. Unknown LTI system with missing data samples

This example considers the unknown LTI system with missing data as presented in [23]. In the first part of this example, we apply Corollary 1 to verify, based only on the available multiple data samples, whether the system is dissipative with respect to a supply function of the form (5) with $N = 0$. This supply and storage functions are found via an optimization procedure that will be discussed further. In the second part, using the system as identified in [23], we generate other trajectories to verify whether the dissipation inequality as in (16), with the supply and storage functions found in the first part of the example, holds in general for a larger interval, i.e., $[0, M]$ with $M \gg L$. This numerical experiment intends to show that the QSR-dissipativity property indeed corresponds to the standard dissipativity with an infinite time horizon.

In [23], the authors consider a measured trajectory obtained from one measurement batch containing missing samples. This trajectory is given as follows

k	0	1	2	3	4	5	6	7	8	9
$y(k)$	3	3	7	6	11	×	18	21	23	24
$u(k)$	1	0	2	−1	0	×	1	1	−1	−5

k	10	11	12	13	14	15	16	17	18	19
$y(k)$	33	31	×	30	20	26	14	10	3	×
$u(k)$	0	−1	×	1	−6	2	−2	0	1	×

where × represents the missing samples. From this information, we can immediately infer that $m = p = 1$, and we can also visualize the three different snapshots of data ($q = 3$), with $T_1 = 5$ and $T_2 = T_3 = 6$. Additionally, in [23], the authors assume the order of the system to be equal to $n = 2$ and a parameter $L = 3$, which we also assume in this paper.

Given this *a priori* information, we can search for a supply function of the form (5) with $N = 0$ and a matrix P as in (11) using Corollary 1 and programming the conditions accordingly. We are indeed able to find the associated quadratic supply-rate function (5) with

$$\Phi_0 = \begin{bmatrix} 0.0011 & 0.0007 \\ 0.0007 & 0.1709 \end{bmatrix}$$

and the associated storage function with

$$P = \begin{bmatrix} 0.084 & -0.140 & 0.061 & -0.138 & 0.123 & -0.061 \\ -0.140 & 0.286 & -0.144 & 0.257 & -0.250 & 0.144 \\ 0.061 & -0.144 & 0.080 & -0.124 & 0.126 & -0.080 \\ -0.138 & 0.257 & -0.124 & 0.340 & -0.216 & 0.124 \\ 0.123 & -0.230 & 0.126 & -0.216 & 0.352 & -0.126 \\ -0.061 & 0.143 & -0.080 & 0.124 & -0.126 & 0.080 \end{bmatrix}.$$

For comparison purposes, we can apply the method presented in [17, Theorem 1] using the available sets containing missing data, assuming the parameters mentioned above and $\nu = 2$, and then searching for a supply rate of the form $\Phi \succeq 0$. Note that for the mentioned method, only (L, ν, N)-QSR-dissipativity[3] is verified; in addition, only the supply rate function is present on the verification, not the storage function. Thus, when applying the search algorithm of [17], we can find the following supply rate

$$\Phi = \begin{bmatrix} 0.3709 & -0.3362 \\ -0.3362 & 0.3709 \end{bmatrix}.$$

We can also verify other methods, namely, [20, Theorem 5], [16], and Theorem 1, to check whether these methods can find a supply function to which the system is dissipative, and a storage function, for Theorem 1. Note, however, that for all these methods, we need to separately apply the three different snapshots from the original data since they do not assume the collective persistence of excitation concept.

For the methods in [20, Theorem 5] and [16], we search for a positive supply function $\Phi \succeq 0$ such that $(L - \nu)$-QSR-dissipativity holds.[4] In both methods [20, Theorem 5] and [16], we need to give a scalar ν to proceed with the search of the supply-rate function. In this example, we apply $\nu = 2$ for the search. Considering both theorems, we cannot find feasible results when checking all three data snapshots separately. This can be explained by the fact that each dataset individually is not persistently excited and because the null matrices that those theorems use do not exist when T is too short. When applying the condition given in Theorem 1 for each dataset separately, we can find matrices P and Φ that satisfy the inequality in (13). However, note that in the latter case, the persistence of excitation is not met; therefore, using such matrices does not imply that the system is dissipative.

To verify whether the dissipative condition in (15) holds with the storage and supply functions previously obtained with Corollary 1 and Theorem 1, we can evaluate (25) using different trajectories. We assume these methods are represented by $Y_1(k)$ and $Y_2(k)$, respectively. For the method in [17, Theorem 1], we verify

$$Y_3(k) := \sum_{k=L}^{1000} w(u(k), y(k)) \geq 0. \tag{35}$$

Using the system model identified in [23], we generate 1000 different trajectories with length $k = 1000$, zero initial conditions and a normally distributed input with a standard deviation of 1 and zero mean. Using these trajectories, we validate whether the dissipativity inequalities described above hold for the whole time interval $k = \{L, 1000\}$.

In Fig. 1 we present the plot of the dissipativity inequalities identified using Corollary 1, Theorem 1, and [17, Theorem 1], represented by $Y_1(k)$, $Y_2(k)$, and $Y_3(k)$, respectively. In this plot, we present the average, minimum and maximum values of $Y_i(k)$ obtained for the set of 1000 different trajectories. The plot of $Y_2(k)$ is obtained using the matrices identified using Theorem 1 with the second measured snapshot, of length T_2.

Fig. 1 shows that, as expected, the dissipative inequality (25) with the matrices identified by Corollary 1 ($Y_1(k)$) holds for all k and for all trajectories tested. The same can be observed with the method from [17, Theorem 1], where it is seen that (35) indeed holds for the whole interval tested. On the other hand, we can see in this figure that using the inequality identified using Theorem 1 with the second measured snapshot, $Y_2(k)$ is positive in some instants k for several trajectories. This is expected since the input of the trajectories used for identifying Φ and P were not persistently exciting, showing that the requirement of the persistence of excitation is indeed necessary. We do not show explicitly the plots of $Y_2(k)$ for the matrices identified using the snapshots T_1 and T_3 since they have similar behaviour as the one shown in Fig. 1.

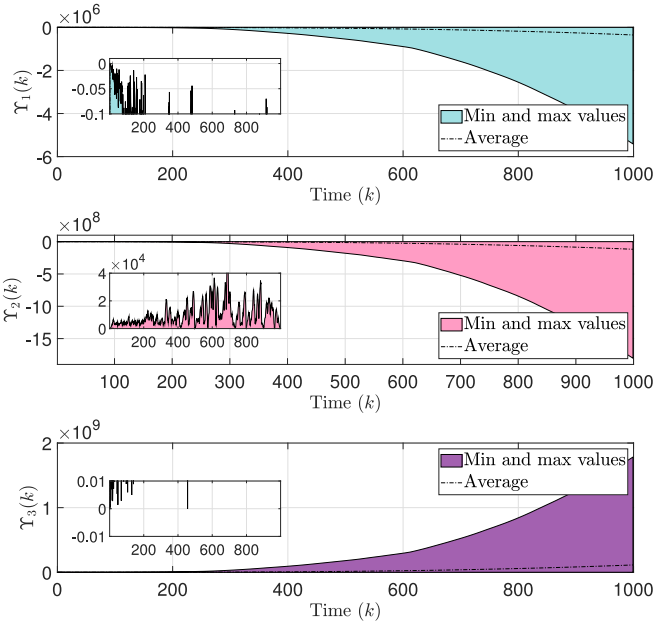

Fig. 1. The plot of $Y_1(k)$ (Corollary 1) and $Y_2(k)$ (Theorem 1, with T_2) as given in (25), with the respective identified supply-rate and storage functions. Additionally, the plot of $Y_3(k)$ ([17, Theorem 1]) with the respective identified supple-rate function.

4.3. Fault detection of a 2 DoF planar manipulator

In this example, we validate our fault detection method by applying it to a two-degree-of-freedom (DoF) planar manipulator from Quanser [28], using a rigid joint configuration as detailed in [29]. This setup can be seen in Fig. 2, where we can see the rigid bars in the joints. In the first part of the example, we identify the dissipative inequality using a shot of data from a fault-free batch of data obtained experimentally on this setup. Later, we apply the fault detection method to several fault cases obtained experimentally.

Regarding the experimental setup, using the rigid joint configuration discussed in [29], the robot can be modelled using a state-space representation where four states represent the generalized positions and momenta of the two joints. Each joint can be actuated with input variables of electrical current (in Amperes) applied to the actuation motors, and we assume the output variables as the generalized position of each joint. For obtaining the fault-free data, we apply a closed-loop system using the controller proposed in Case 2 of Section 5.1 of [29], in which the robot is operated in the neighbourhood of generalized positions $q^* = \begin{bmatrix}0.6 & 0.8\end{bmatrix}^\top$ and generalized momenta $p^* = \begin{bmatrix}0 & 0\end{bmatrix}^\top$ so that the dynamics can be approximated by an LTI system (3). Additionally, for exciting the input, we consider an external signal with a normal distribution, a standard deviation of 0.05 and zero mean that is calculated and applied separately to each of the joints. The time-series input–output data is collected with a sampling time of $T_s = 0.005$s. A block diagram of the experimental setup is shown in Fig. 3.

Fig. 4 shows the data from one of the experiments where we can see that the robots operate in the neighbourhood of (q^*, p^*). Note that we

[3] (L, ν, N)-QSR-dissipativity is a relaxed version of the QSR-dissipativity, in which the supply-rate function is verified on a finite-time interval of $[0, L - \nu - 1]$, instead of $[0, \infty]$, which is equivalent to the general notion of dissipativity.

[4] Similarly to the (L, ν, N)-QSR-dissipativity, the $(L - \nu)$-QSR-dissipativity is a relaxed version of the QSR-dissipativity, in which the supply function is verified on a finite-time interval of $[0, L - 1]$, with the first $[0, \nu]$ instants being equal to zero.

Fig. 2. 2 DoF planar manipulator from Quanser.

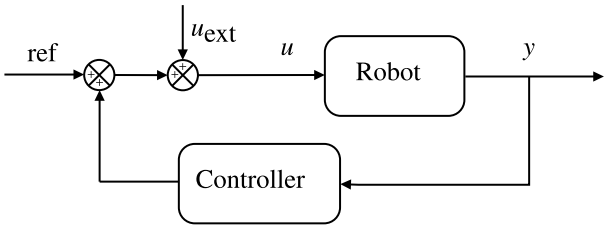

Fig. 3. Schematic of the experimental setup.

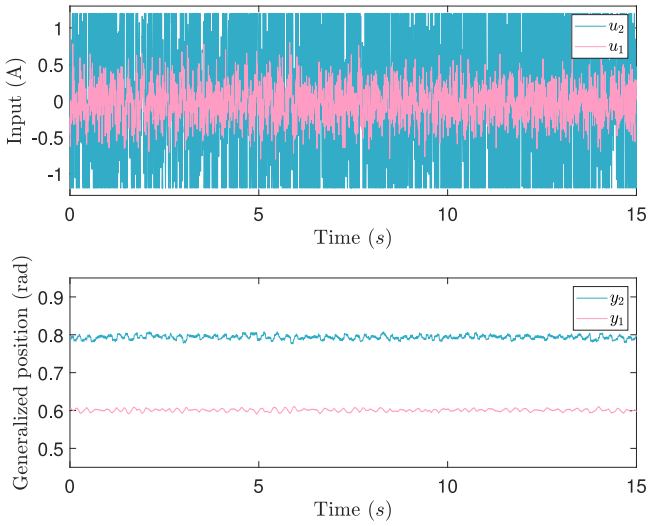

Fig. 4. One set of experimental data of a 2-DoF planar manipulator from Quanser. The closed-loop system (robot + controller) operates at an equilibrium point $(q^*, p^*) = (\begin{bmatrix}0.6\\0.8\end{bmatrix}, \begin{bmatrix}0\\0\end{bmatrix})$ while perturbed by an external signal.

do not include the transient time, instead, we consider the input–output data of the robot already stabilized. This experiment can be found in form of a video at youtu.be/2kg4Tp3qp3Y.

In this example, we consider the data obtained in the experiment shown in Fig. 4 for identifying the dissipative inequality (25). We take $N = 1$, $L = 4$ and $T = (m+1)(L+n) + m(N+1) = 28$ samples. The snapshots then have the form of $(u_{[0,T+N-1]}, y_{[0,T+N-1]})$ and are obtained from a window starting at 1s. Note, however, that we can choose this interval to start at any point of the batch of experiments in which the robot is already stabilized. The choice of $L = 4$ comes from the knowledge of the order of the system and $N = 1$ given that we know that any robotic manipulator is dissipative with respect to the QdF supply-rate function of $w(u(t), y(t)) = \dot{y}(t)^\top u(t)$ (in the continuous-time case) or its associated discrete-time version $w(u_{[\cdot,\cdot+1]}, y_{[\cdot,\cdot+1]}) = (y(k+1) - y(k))^\top u(k+1)$. Thus, we choose a QdF that includes both $y(k+1)$ and $y(k)$. Using these parameters, we can search for and find a feasible solution of P and Φ using Theorem 1.

With the identified dissipative inequality in hands, we can construct the residual function as in 27 and apply it to the fault detection case. We assume several kinds of faults caused manually after the time instant of 5s but not directly after 5s. They are: (i) holding the robot manually; (ii) a gain representing an increase of 50% in the applied input; (iii) removal of the rigid bar on link 1; (iv) removal of the rigid bar on the link 2; and (v) removal of the rigid bars on both links 1 and 2. Removing the rigid bar makes the robot operate with a flexible configuration, which is not considered in the control configuration we are applying. A video of this experiment can be found at youtu.be/CeRoGj1nRHY.

Before we present the fault detection results, we can analyse the behaviour of the dissipative inequality as in $Y(k)$. In Fig. 5, we present the plot of $Y(k)$ for the five different faulty cases. For obtaining this plot, the function $Y(k)$ uses the matrices P and Φ that are identified using Theorem 1 with the parameters described before and a small window of data from the trajectory of the fault-free case. Note that for all faulty cases, the dissipativity properties still hold, that is, $Y(k) \leq 0$ for all instants tested. Thus, as we mentioned in Section 3, the use of this dissipative inequality (25) as a method for verifying the presence of a fault would not be able to detect any of the faults that we show in this paper.

Hence, we verify the residual function $J(k)$ as in 27 with the following choices of parameters: $T_{\text{F}} = 150$, $\beta = 1.1$, representing a margin of 10% more than the largest magnitude value of the residual function of the nominal case, and $\gamma = 3$, considering $J_{[0,T_{\text{TH}}]}$ to be normally distributed. Using these parameters and the data from the fault-free case, we obtain $\text{TH}_\beta = 50.9925$ and $\text{TH}_\gamma = 49.6243$.

In Fig. 6, we have the plot of the evaluation function $J(k)$ as in 27 applied to the fault-free and faulty experiments using $Y(k)$ with the matrices identified previously. Note that in the cases of faults (i) and (ii)–(v), the evaluation function crosses both thresholds in the presence of the fault during the whole time that there is a fault in the system.

In the case where we represent a failure in the input, i.e. fault (ii), the evaluation function shows the presence of a fault for some parts of the trajectory but not during the entire period where there is a fault (in this case, we apply the fault directly from time instant 5s). This can be explained by the safety procedure that saturates the input control. Meaning that even if we force the increase in the input, the system will saturate this signal. If this step is not considered, we can permanently damage the system, which is not our goal. As shown in Fig. 4, the signal applied to the motor in the second link is already saturating in most of the trajectory during the nominal condition. Thus, the input increase will not influence the behaviour much, at least for this link. On the other hand, for the first link, we have a higher margin of increase in the control actuation. This increase is considered in the feedback loop and can eventually stabilize the system.

The results in Fig. 6 show that we can detect faults, even when their effects in the system are minimum, as in the case of fault (ii). Note also, that the thresholds TH_β and TH_γ, as we designed, provide similar

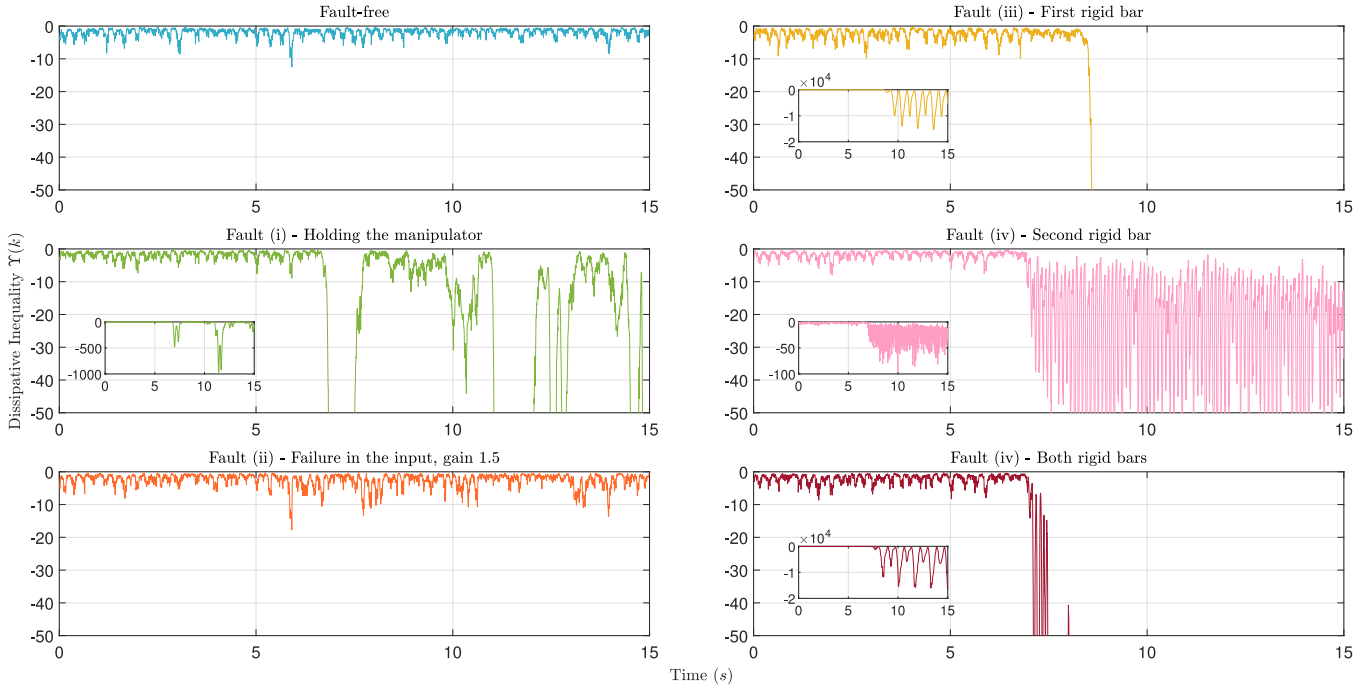

Fig. 5. The plot of $\Upsilon(k)$ for several experiments, where $\Upsilon(k)$ is of the form of (25), where the matrices P and Φ are identified using a trajectory from the fault-free experiment.

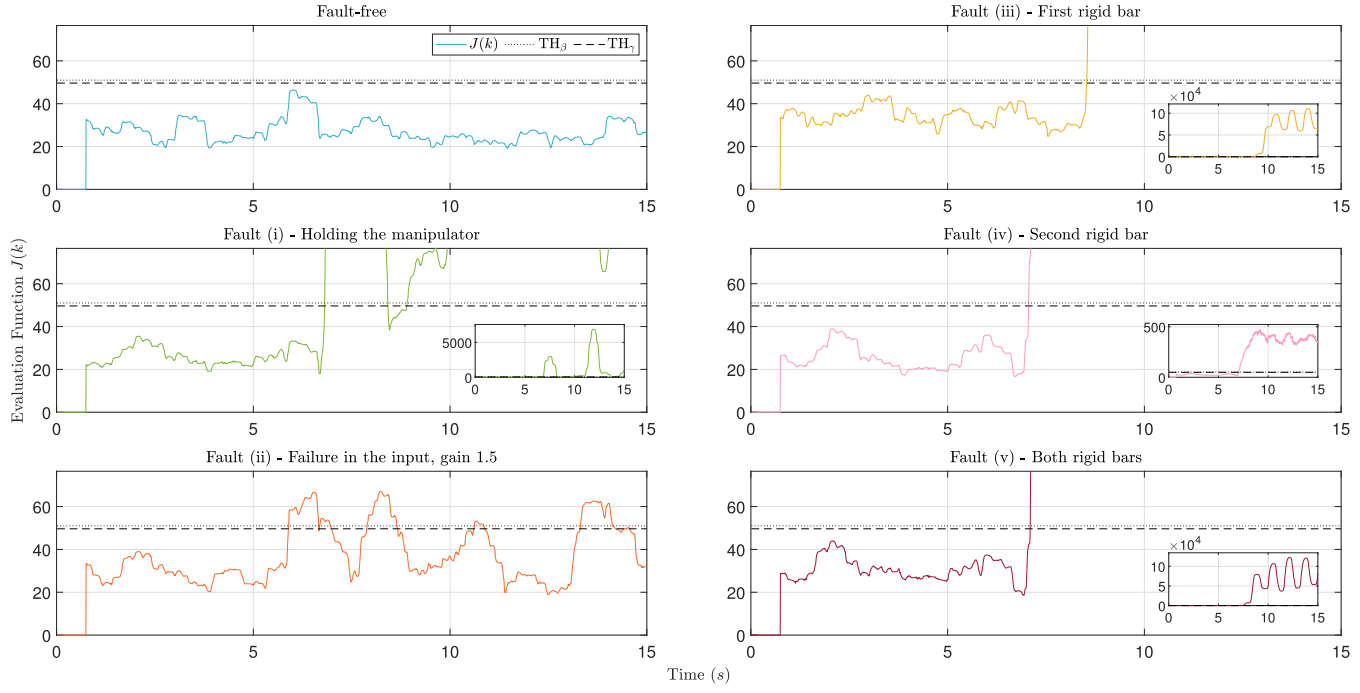

Fig. 6. The plot of the evaluation function $J(k)$ for several experiments, including the fault-free experiment used to identify $\Upsilon(k)$. Note that the thresholds TH_β and TH_γ are represented by : and −− respectively.

results. In the presence of a fault, both are effective in detecting the faults. If we had tuned, for instance, β as a lower percentage margin, we would trigger more faults, or, in the case where β corresponds to a higher margin, it would not be able to detect all faults. The same interpretation is application to the parameter γ. This shows the importance of tuning these parameters in the design phase of the implementation of the technique.

We compare our fault detection method to a PCA (Principal Component Analysis) method. For that, we use only the measured output signals as the input data for this algorithm since the PCA approach is

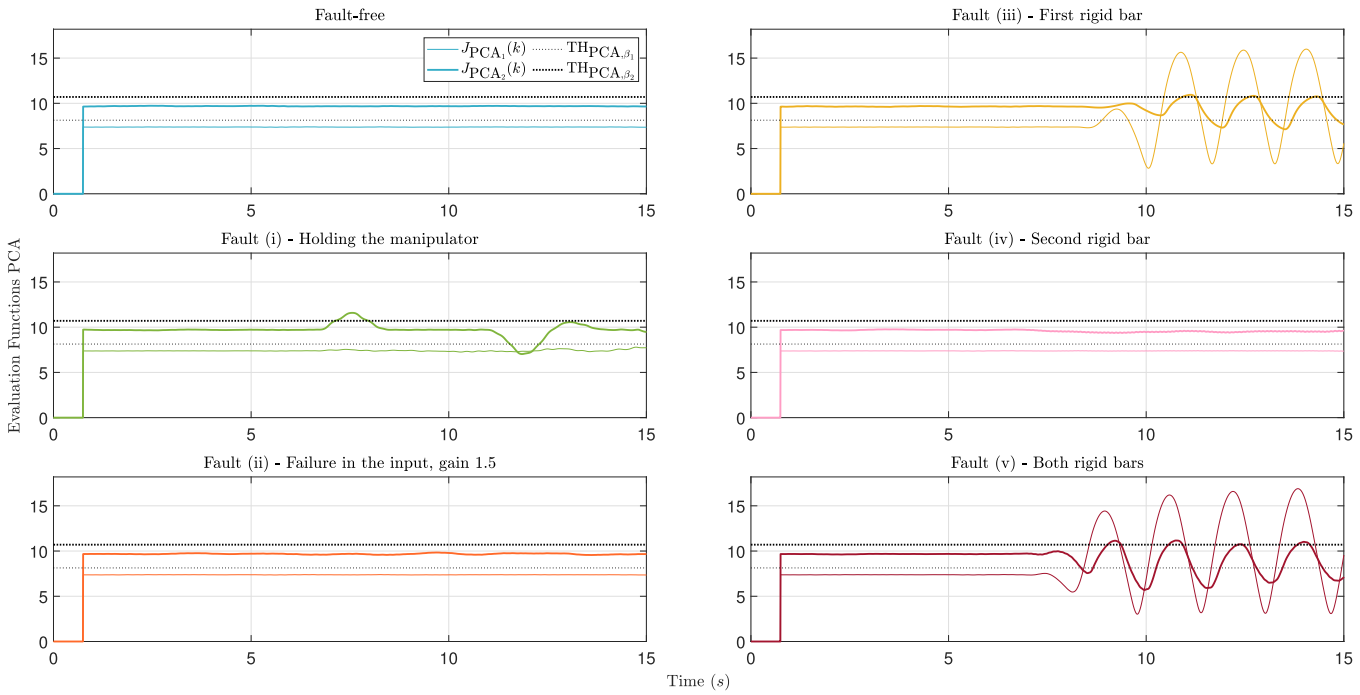

Fig. 7. The result of fault detection using principal component analysis method using the evaluation functions J_{PCA_1} and J_{PCA_2} for the same experimental data as before. Note that the thresholds $\text{TH}_{\text{PCA},\beta_1}$ and $\text{TH}_{\text{PCA},\beta_2}$ are represented by : and −− respectively. Note that the numbering 1 and 2 is related to the first and second joint signals, or y_1 and y_2.

based on the correlation between the analysed variables. Since we do not vary the input significantly in the nominal case in this example, we will not be able to see a strong correlation to the input. For obtaining a residual function, we apply a similar method to the one explained in [30], using the principal components score plot, also called T2. We use the Matlab function `pca`, using the inverse of variances of the ingredients as variable weight and the principal component coefficients matrix to obtain the residual function. In other words, we have

$$r_{\text{PCA}}(k) = y(k) - P_{\text{PCA}}y(k);$$

where P_{PCA} is the principal component coefficients matrix and $r_{\text{PCA}}(k)$ is the residual function. We obtain the matrix P_{PCA} by applying the function `pca` to the same fault-free trajectory used with our method and use this same P_{PCA} to verify the residual values in the fault detection online algorithm.

Since the data we used in the PCA algorithm comprises the signals of the two joints, we have residual values related to each. Thus, we can obtain evaluation functions J_{PCA_1} and J_{PCA_2}, related respectively, to the first and second joint signals y_1 and y_2. The evaluation functions are as given in 27, where we assume the squared root of the norm of the residue $r(k)$. We also consider the same T_F as we used for our method, that is, $T_F = 150$.

We can obtain the threshold values using the idea proposed in Section 3. We apply the same parameters we used for our method, $\beta = 1.1$ and $\gamma = 3$. Using (29), we obtain $\text{TH}_{\text{PCA},\beta_1} = 8.1340$ and $\text{TH}_{\text{PCA},\beta_2} = 10.7024$, which corresponds to the thresholds for joints 1 and 2, respectively. Using (30), these values are equal to $\text{TH}_{\text{PCA},\gamma_1} = 11.8315$ and $\text{TH}_{\text{PCA},\gamma_2} = 15.5347$, for joints 1 and 2, respectively.

In Fig. 7, we show the results of applying the evaluation functions J_{PCA_1} and J_{PCA_2}, where the residual function is obtained with the PCA method and which function is related, respectively, to the first and second joints. For easier visualization, we have omitted the thresholds obtained as in (30) in Fig. 7 since the obtained threshold values are higher than the ones obtained as in (29).

As we can see in Fig. 7, the PCA method is only able to detect part of the faults for the cases (i), (iii) and (v), which can be seen when the evaluation function crosses the thresholds. However, the method does not detect the fault presence for most of the faulty trajectories. Let us compare the signals related to the first and second joints, y_1 and y_2. For cases (iii) and (v), we see that the first evaluation function detects the fault in the first rigid bar for part of the trajectory, while the second does not always detect it. However, as we can see in the data from the experiments shown in the aforementioned YouTube video, both links are affected in these cases. In case (i), we see the opposite, the evaluation function related to the second joint can briefly detect a fault. In contrast, both evaluation functions do not detect faults during the remainder of the trajectory. For cases (ii) and (iv), the method cannot detect any faults in these experiments.

Table 1
Time of the first detected faults using the thresholds obtained for Algorithm 1 and for the PCA approach.

Fault	TH_{β}	TH_{γ}	$\text{TH}_{\text{PCA},\beta_1}$	$\text{TH}_{\text{PCA},\beta_2}$	$\text{TH}_{\text{PCA},\gamma_1}$
(i)	6.815	6.815	–	7.130	–
(ii)	5.900	5.895	–	–	–
(iii)	7.100	7.100	8.425	9.030	8.625
(iv)	8.540	8.535	8.885	10.915	10.505
(v)	7.060	7.060	–	–	–

Comparing the results in Figs. 6 and 7, we see that even though our method cannot directly be used for fault isolation, that is, identifying in which signal the fault is present, our method provides a better detection than the PCA method. Note that both methods were offline trained using the same fault-free trajectory and applying the same evaluation procedure concerning the residue signals.

In Table 1, we provide the time instant (in seconds) of the first fault detection using our method and the PCA approach. We have omitted the column regarding the results obtained using the threshold $\text{TH}_{\text{PCA},\gamma_2}$ since no fault in the second link was detected using it. From Table 1, we can see that our method was able to detect the faults faster than the compared method for all studied fault trajectories. With regard to the proposed method, we can see that there is little to no difference in this parameter considering the use of the threshold values TH_{β} and TH_{γ}, which shows that the design we perform provides similar results.

5. Conclusions

This paper tackled the fault detection problem using dissipativity analysis as a base. The first main novelty we provided was a new method to verify the dissipativity of an LTI system using only one or multiple shots of data considering a QdF form of the supply rate function. From this result, we developed a new fault detection method where the norm of the dissipativity inequality works as an evaluation function. In order to illustrate the applicability of the theoretical results, we presented a set of simulations comparing our results with the methods in [16,17,20]. Furthermore, an implementation using a two-degree-of-freedom planar manipulator was also provided, where we applied the method introduced in this paper and a PCA method, for comparison purposes. The planar manipulator was subjected to several types of faults, and as described in the results, all faults were detected when applying our method. Using the PCA approach, not all faults were detected and also not for the entire faulty trajectory. Another important aspect was the results obtained for the fault-free case, where not a single incidence of missed fault detection occurred during the experiment when applying our method. The aforementioned results show that the proposed solution is a fit approach for fault detection, especially for cases where the mathematical models, due to high complexity and data-driven, which require much data, are not implementable.

CRediT authorship contribution statement

Tábitha E. Rosa: Conceptualization, Methodology, Software, Investigation, Writing – original draft. **Leonardo de Paula Carvalho:** Conceptualization, Software, Writing – review & editing. **Gabriel A. Gleizer:** Writing – review & editing. **Bayu Jayawardhana:** Supervision, Conceptualization.

Declaration of competing interest

The authors declare the following financial interests/personal relationships which may be considered as potential competing interests: Tabitha E. Rosa reports financial support was provided by Dutch Research Council (NWO). Gabriel A. Gleizer reports financial support was provided by Dutch Research Council (NWO).

Data availability

Data will be made available on request.

Acknowledgement

This publication is part of the project Digital Twin projects 0 and 4, with project number P18-03, of the research programme Perspectief which is (mainly) financed by the Dutch Research Council (NWO).

References

[1] Chen J, Patton RJ. Robust model-based fault diagnosis for dynamic systems, vol. 3. Springer Science & Business Media; 2012.
[2] Isermann R. Fault-diagnosis systems: An introduction from fault detection to fault tolerance. Springer Science & Business Media; 2005.
[3] Patton RJ, Frank PM, Clark RN. Issues of fault diagnosis for dynamic systems. Springer Science & Business Media; 2000.
[4] Nor NM, Hassan CRC, Hussain MA. A review of data-driven fault detection and diagnosis methods: Applications in chemical process systems. Rev Chem Eng 2020;36(4):513–53.
[5] Jiang K, Kheradmandi M, Hu C, Pal S, Yan F. Data-driven fault tolerant predictive control for temperature regulation in data center with rack-based cooling architecture. Mechatronics 2021;79:102633.
[6] da Silva GM, Pederiva R. Fault diagnosis of active magnetic bearings. Mechatronics 2022;84:102801.
[7] Willems JC. Dissipative dynamical systems part I: General theory. Arch Rational Mech Anal 1972;45(5):321–51.
[8] Lei Q, Munir MT, Bao J, Young B. A data-driven fault detection method based on dissipative trajectories. IFAC-PapersOnLine 2016;49(7):717–22.
[9] Li W, Yan Y, Bao J. Data-based fault diagnosis via dissipativity-shaping. IEEE Control Syst Lett 2022;7:484–9.
[10] Rotulo M, De Persis C, Tesi P. Online learning of data-driven controllers for unknown switched linear systems. Automatica 2022;145:110519.
[11] De Persis C, Tesi P. Formulas for data-driven control: Stabilization, optimality, and robustness. IEEE Trans Automat Control 2019;65(3):909–24.
[12] Tang W, Daoutidis P. Dissipativity learning control (DLC): A framework of input–output data-driven control. Comput Chem Eng 2019;130:106576.
[13] Lei Q, Bao J. Dissipativity based fault detection and diagnosis for linear systems. In: 2015 IEEE conference on control applications. IEEE; 2015, p. 133–8.
[14] Li W, Bao J, Wei G. A new fault detection method from data-based dissipativity theory. In: 2021 40th Chinese control conference. IEEE; 2021, p. 4579–84.
[15] Koch A, Berberich J, Allgower F. Provably robust verification of dissipativity properties from data. IEEE Trans Automat Control 2021.
[16] Rosa TE, Jayawardhana B. On the one-shot data-driven verification of dissipativity of LTI systems with general quadratic supply rate function. In: Proc. 19th European control conf.. Rotterdam: IEEE; 2021, p. 1291–6.
[17] Rosa TE, Jayawardhana B. Data-driven dissipative verification of LTI systems: Multiple shots of data, QDF supply-rate and application to a planar manipulator. In: 16th European workshop on advanced control and diagnosis.
[18] Willems J, Trentelman H. On quadratic differential forms. SIAM J Control Optim 1998;36(5):1703–49.
[19] Trentelman H, Willems J. Every storage function is a state function. Syst Control Lett 1997;32(5):249–59.
[20] Romer A, Berberich J, Köhler J, Allgöwer F. One-shot verification of dissipativity properties from input–output data. IEEE Control Syst Lett 2019;3(3):709–14.
[21] Willems JC, Rapisarda P, Markovsky I, De Moor BL. A note on persistency of excitation. Syst Control Lett 2005;54(4):325–9.
[22] Dresscher M, Jayawardhana B, Kooi B, Scherpen J. Toward observable UHVCVD: Modeling of flow dynamics and AAS partial pressure measurement implementation. Mechatronics 2020;71:102427.
[23] van Waarde HJ, De Persis C, Camlibel MK, Tesi P. Willems' fundamental lemma for state-space systems and its extension to multiple datasets. IEEE Control Syst Lett 2020;4(3):602–7.
[24] Brogliato B, Lozano R, Maschke B, Egeland O. Dissipative systems analysis and control: Theory and applications, vol. 2. Springer; 2007.
[25] Moylan P. Dissipative systems and stability.
[26] Löfberg J. YALMIP: A toolbox for modeling and optimization in MATLAB. Taipei, Taiwan; 2004, p. 284–9.
[27] MOSEK ApS. The MOSEK optimization toolbox for MATLAB manual. Version 9.0.. 2019.
[28] Quanser. 2 DOF serial flexible joint, reference manual. Doc. No. 800, rev 1. 2013.
[29] Chan-Zheng C, Borja P, Scherpen JM. Passivity-based control of mechanical systems with linear damping identification. IFAC-PapersOnLine 2021;54(19):255–60.
[30] Mnassri B, El Adel EM, Ananou B, Ouladsine M. Fault detection and diagnosis based on PCA and a new contribution plot. IFAC Proc Vol 2009;42(8):834–9, 7th IFAC Symposium on Fault Detection, Supervision and Safety of Technical Processes.

Tabitha E. Rosa received her Ph.D. from the University of Groningen, The Netherlands in 2023, her Master degree in Electrical Engineering at Universidade Estadual de Campinas (UNICAMP) in 2017, and a Bachelor degree in Mechatronics Engineering at Centro Federal de Educação Tecnológica de Minas Gerais (CEFET-MG) in 2014. She is currently a mechatronics design engineer at ASML Netherlands. Her interests include robust control, convex optimization, linear time-invariant and parameter varying systems, data-driven analysis, dissipativity, and fault diagnosis.

Leonardo de Paula Carvalho is currently a Postdoctoral Associate at Yale School of Medicine, USA. He received his Double Ph.D. in Electrical Engineering at the University of São Paulo, Brazil (2022), and the University of Groningen, The Netherlands. He received his Master's in Electrical Engineering at the State University of Campinas (UNICAMP), Brazil (2016), and a Bachelor's in Electrical Engineering at the Federal University of Mato Grosso do Sul (UFMS), Brazil (2012). His research interests include machine learning, control, and filtering theory, fault detection, fault-tolerant control, convex optimization, Markov jump linear systems, networked control systems, Linear Parameter Varying, and data-driven control.

Gabriel de A. Gleizer is a postdoctoral researcher at the Delft Center for Systems and Control (DCSC), Delft University of Technology (The Netherlands). He received his Control and Automation Engineering degree in 2010 and his M.Sc. in Electrical Engineering in 2013 from the Federal University of Rio de Janeiro, Brazil, and his Ph.D. (cum laude) in Systems and Control also in DCSC, TU Delft. Before his Ph.D., he was a Research Engineer at GE Global Research in Rio de Janeiro, from 2012 to 2017. His main research interests are hybrid systems, fault diagnosis, networked control systems, and formal methods for (quantitative) analysis and control.

Bayu Jayawardhana (SM'13) received the B.Sc. degree in electrical and electronics engineering from the Institut Teknologi Bandung, Bandung, Indonesia, in 2000, the M.Eng. degree in electrical and electronics engineering from the Nanyang Technological University, Singapore, in 2003, and the Ph.D. degree in electrical and electronics engineering from Imperial College London, London, U.K., in 2006. He is currently a professor of mechatronics and control of nonlinear systems in the Faculty of Science and Engineering, University of Groningen, Groningen, The Netherlands. He was with Bath University, Bath, U.K., and with University of Manchester, Manchester, U.K. His research interests include the analysis of nonlinear systems, systems with hysteresis, mechatronics, robotics and systems biology.